Hindawi Publishing Corporation
EURASIP Journal on Wireless Communications and Networking
Volume 2008, Article ID 586172, 14 pages
doi:10.1155/2008/586172

Research Article

Cyclostationarity-Inducing Transmission Methods for Recognition among OFDM-Based Systems

Koji Maeda, Anass Benjebbour, Takahiro Asai, Tatsuo Furuno, and Tomoyuki Ohya

Research Laboratories, NTT DoCoMo, Inc., 3–5 Hikari-no-oka, Yokosuka, Kanagawa 239-8536, Japan

Correspondence should be addressed to Koji Maeda, maedakou@nttdocomo.co.jp

Received 29 June 2007; Revised 14 December 2007; Accepted 18 March 2008

Recommended by Ivan Cosovic

This paper proposes two cyclostationarity-inducing transmission methods that enable the receiver to distinguish among different systems that use a common orthogonal frequency division multiplexing- (OFDM-) based air interface. Specifically, the OFDM signal is configured before transmission such that its cyclic autocorrelation function (CAF) has peaks at certain preselected cycle frequencies. The first proposed method inserts a specific preamble where only a selected subset of subcarriers is used for transmission. The second proposed method dedicates a few subcarriers in the OFDM frame to transmit specific signals that are designed so that the whole frame exhibits cyclostationarity at preselected cycle frequencies. The detection probabilities for the proposed cyclostationarity-inducing transmission methods are evaluated based on computer simulation when optimum and suboptimum detectors are used at the receiver.

1. INTRODUCTION

In recent years, cognitive radio has attracted much attention as a key solution towards accommodating several wireless communication systems in the same frequency band [1–3]. Cognitive radio devices are equipped with the capability to sense the radio environment and then adaptively configure their transmission parameters, for example, carrier frequency, baud rate, and beam-forming pattern, according to the sensing results and the spectrum utilization policies [4, 5]. In a spectrum-sharing scenario where the secondary usage of underutilized spectrum portions, that is, white space, of a primary system is allowed, secondary systems are able to acquire free spectrum by opportunistically accessing the white space of the primary system [6]. Nevertheless, a secondary cognitive user, before transmission, needs to sense the spectrum and confirm the absence of primary users in order to avoid imparting harmful interference to those users [7]. Recognition among multiple secondary systems competing for white space spectrum is also important as it may enable the setting of advanced spectrum policy such as multilevel priority or advanced access control such as maintaining fairness among secondary systems [8].

Recognition of primary users is generally performed under the constraint of limited information pertaining to the characteristics of the signals transmitted by primary users [2, 3]; therefore, feature detection is widely employed for this purpose. Feature detection, being superior to energy detection and inferior to optimum matched-filter detection [7, 9], has the advantage of detecting signals based solely on their statistical properties, for example, second-order cyclostationarity and higher-order statistics [2, 10–13]. Such properties are generally related to the signal structure owing to the air interface, for example, transmission symbol rate and carrier frequency.

On the other hand, when the recognition among multiple secondary systems is required in addition to the recognition of the primary system, only matched filter and feature detections are applicable, and energy detection cannot be utilized since it can only detect whether a signal is present within the frequency band of interest, and not the system to which the signal belongs.

For the recognition of primary and secondary systems, therefore, the following two types of detectors can be considered.

(1) A hybrid detector that, after recognizing the absence of the primary system, uses matched-filter detection to differentiate among secondary systems.
(2) A unified detector that, based solely on feature detection, simultaneously differentiates between primary and secondary systems and among secondary systems.

Both detectors, however, have their own issues. For the hybrid detector, how to define decision regions and unify decision criteria for two different types of detectors, that is, statistical feature and matched-filter detection, arise as a problem. In addition, and more importantly, a lesser degree of flexibility is applicable among secondary systems since their matched filter detectors require knowledge regarding some of their actually transmitted signal sequences.

In recent years, orthogonal frequency division multiplexing (OFDM) is becoming the air interface of choice for several wireless standards, and the probability that the secondary systems will choose the OFDM-based air interface is increasing. Consequently, for the unified detector, an important issue is how to configure flexibly the transmit signals of secondary systems such that their features are made different than the primary system and different among secondary systems, even when the same air interface is used. In this paper, we focus on the unified detector and study feature-inducing transmission methods that enable the receiver to distinguish among multiple secondary systems that use OFDM as a common air interface. As a signal feature, we choose second-order cyclostationarity, which has lower computational complexity compared to other feature detectors that are based on higher-order statistics.

A signal is said to exhibit cyclostationarity if its cyclic autocorrelation function (CAF) is nonzero for a nonzero cycle frequency. A cyclostationarity-inducing transmission method was previously studied in the context of blind channel equalization for single-carrier transmission [14]. This method can be easily extended to the context of signal recognition, but cannot be applied to OFDM-based systems. For OFDM signals, the inherent cyclostationarity owing to guard interval (GI) can be easily exploited for recognition among multiple OFDM-based systems if the length of the GI in each OFDM-based system is appropriately assigned. In this case, however, the frame length of OFDM signals is not fixed and varies from a system to another according to the assigned length of the GI for every system. To induce cyclostationarity in OFDM signals under a fixed frame length and identical parameters for all systems to be recognized, we propose in this paper two different methods of configuring the OFDM signal before transmission such that the CAF is nonzero at certain preselected cycle frequencies. The first proposed method inserts a specific preamble at the beginning of an OFDM frame. Each preamble is configured such that only a selected subset of subcarriers is used for transmission. A different subset of subcarriers results in the occurrence of CAF peaks at different cycle frequencies for the OFDM signal. The second proposed method is based on dedicating a few subcarriers at each OFDM symbol to the transmission of specific signals so that the whole OFDM frame comprising several OFDM symbols exhibits cyclostationarity at preselected cycle frequencies. For this method, we introduce a method for generating signals on the dedicated subcarriers and describe their relation to the cycle frequencies of the configured OFDM frame.

On the receiver side, for system recognition, the CAFs for the received signals are compared to the CAF candidates calculated and stored in advance for the systems to be distinguished. For this purpose, a minimum distance detector [15, 16] is employed in the CAF domain. The minimum distance detector gives the optimum detector when the prior probabilities of transmission for all systems are equal. Nevertheless, it requires the channel state information (CSI) corresponding to the received signal. However, in a spectrum-sharing scenario, the assumption of known CSI is usually not practical. Therefore, a suboptimum detector that does not require CSI is also introduced and discussed. The detection probabilities when using the proposed methods to induce cyclostationarity at the transmitter are evaluated based on computer simulation. Results are given for both AWGN and multipath Rayleigh fading channels and when both optimum and suboptimum detectors are used at the receiver.

This paper is organized as follows. First, in Section 2, we introduce the concept of second-order cyclostationarity. In Section 3, following the description of the mathematical formulation of OFDM signals, both proposed cyclostationarity-inducing transmission methods are presented. In Section 4, the optimum and suboptimum detectors used at the receiver are presented. The performance evaluation results are shown in Section 5. After assessment and discussion regarding the overhead in the proposed methods, the paper is concluded in Section 7.

2. CONCEPT OF SECOND-ORDER CYCLOSTATIONARITY

Let $x(t)$ be a complex signal. The CAF for a complex signal, $x(t)$, is defined as follows [10]:

$$R_x^{\alpha}(\tau) = \lim_{T\to\infty} \frac{1}{T} \int_{-T/2}^{T/2} x\left(t - \frac{\tau}{2}\right) x^*\left(t + \frac{\tau}{2}\right) e^{-j2\pi\alpha t} dt, \quad (1)$$

where $*$ denotes conjugation. When $R_x^{\alpha}(\tau) \neq 0$ for $\alpha \neq 0$, α is said to be the cycle frequency of $x(t)$ at lag parameter τ, and $x(t)$ is said to exhibit second-order cyclostationarity.

Hereafter, the following discrete time version of the consistent estimator of (1) is used:

$$\widetilde{R}_x^{\alpha}[\nu] = \frac{1}{I_0} \sum_{i=0}^{I_0-1} x[i] x^*[i+\nu] e^{-j2\pi\alpha i T_s}, \quad (2)$$

where ν is the discrete version of lag parameter τ, I_0 is the observation interval, and $x[i] = x(iT_s)$, where T_s is the sampling time.

Here, using a Fourier series, a complex signal, $x[i]$, can be expressed by

$$x[i] = \sum_f X_f e^{j2\pi f i T_s}, \quad (3)$$

where X_f is the Fourier coefficient of $x[i]$. By substituting (3) into (2),

$$\widetilde{R}_x^{\alpha}[\nu] = \sum_{f_1} \sum_{f_2} X_{f_1} X_{f_2}^* \epsilon(f_1 - f_2 - \alpha, I_0) e^{-j2\pi f_2 \nu T_s}, \quad (4)$$

where $\epsilon(f, I_0) = (1/I_0)\sum_{i=0}^{I_0-1} e^{j2\pi f i T_s}$. Here, when I_0 approaches infinity,

$$\epsilon(f_1 - f_2 - \alpha, I_0) = \begin{cases} 1, & f_1 - f_2 - \alpha = \dfrac{d}{T_s}, \\ 0, & \text{otherwise}, \end{cases} \tag{5}$$

where d is an integer. Therefore, (5) becomes nonzero only at $\alpha = f_1 - f_2 - d/T_s$. On the other hand, from (2), the CAF for $\alpha = \alpha_0$ and that for $\alpha = \alpha_0 + a/T_s$ ($a \in \mathbf{Z}$) are equivalent. Therefore, we can simply focus on the case of $d = 0$. Accordingly, when I_0 approaches infinity, (4) can be rewritten as

$$\widetilde{R}_x^{\alpha}[\nu] = \sum_f X_f X_{f-\alpha}^* e^{-j2\pi(f-\alpha)\nu T_s}. \tag{6}$$

Note that when $\nu = 0$ in (6), the CAF simply takes the form of the spectral correlation for signal $x[i]$. The cycle frequencies at which the CAF shows peaks is known to differ from one signal to another depending on the time-frequency statistical structure of these signals, which is generally related to the air interface parameters such as the modulation scheme and the baud rate [12].

3. CYCLOSTATIONARITY-INDUCING TRANSMISSION METHODS FOR OFDM-BASED SYSTEM RECOGNITION

In this section, we consider methods to induce artificially at the transmitter different cyclostationarity properties in different OFDM-based systems.

First, let us briefly review the mathematical formulation of general OFDM signals. A discrete version of an OFDM signal can be represented by

$$x[i] = \sum_{\nu=0}^{V-1}\sum_{k=0}^{K-1} s_k[\nu] u\left[\frac{i}{N} - \nu\right] e^{j2\pi k\Delta f i T_s}, \tag{7}$$

where $s_k[\nu]$ is the νth transmitted symbol on the kth subcarrier, K is the number of subcarriers used in an OFDM signal, Δf is the subcarrier frequency spacing, V is the number of OFDM symbols in an OFDM frame, and N is the size of the DFT used. Therefore, $NT_s = 1/\Delta f$ is the OFDM symbol duration. Term $u[\ell]$ is the rectangular function, which is given by

$$u[\ell] = \begin{cases} 1, & 0 \le \ell < 1, \\ 0, & \text{otherwise}, \end{cases} \tag{8}$$

Here, by additionally including the GI, the OFDM signal is represented by

$$x[i] = \sum_{\nu=0}^{V-1}\sum_{k=0}^{K-1} s_k[\nu] u\left[\frac{i}{N_{\mathrm{dg}}} - \nu\right] e^{j2\pi k\Delta f(i-\nu N_{\mathrm{dg}})T_s}, \tag{9}$$

where $N_{\mathrm{dg}} = N + N_g$ and N_g is the length of the GI.

Here, it is well known that, due to the GI, the CAF for the OFDM signals shows peaks for $\nu = \pm N$ and $\alpha = d_n/N_{\mathrm{dg}}T_s$, where $d_n \in \mathbf{Z}$ [2, 12]. However, in this paper, the data and GI lengths are fixed; thus, the CAF peaks owing to the GI cannot be exploited since they are identical for all OFDM-based systems to be recognized. In the following, to induce cyclostationarity in OFDM signals so that signal recognition is possible even when the GI and other radio transmission parameters are the same, we propose two methods A and B.

3.1. Method A: Cyclostationarity-inducing transmission method by inserting specific preambles

Method A is based on the insertion of a specific preamble that has the frequency-domain characteristics configured. The preamble is inserted at the beginning of an OFDM frame, and only a selected subset of subcarriers is used for transmission. More specifically, in (7) or (9), the symbols transmitted on the selected subset of subcarriers, $s_{k\in G}[i]$, are nonzero, and those on the remaining subcarriers, $s_{k\notin G}[i]$, are set to zero where G denotes the selected subset. For a preamble that comprises V_0 symbols, the transmitter keeps transmitting the same symbol, s_k, over V_0 successive OFDM symbols over the selected subset of subcarriers.

For the case when the preamble part contains no GI, from (7), for sufficiently large V_0, the frequency representation of the preamble can be written as

$$X_f = \begin{cases} s_k, & f = k\Delta f,\ k \in G, \\ 0, & \text{otherwise}. \end{cases} \tag{10}$$

Based on (6) and (10), the CAF for the OFDM signal is obtained for $\alpha = n\Delta f$ as

$$\widetilde{R}_x^{n\Delta f}[\nu] = \sum_{k=0}^{K-1} s_k s_{k-n}^* e^{-j2\pi((k-n)\Delta f)\nu T_s}. \tag{11}$$

This is because the frequency component of the OFDM signal is nonzero only at $f = k\Delta f$ for sufficiently large V_0. Equation (11) means that the CAF of an OFDM signal for $\alpha = n\Delta f$ becomes the correlation between the transmitted signal and its n subcarrier frequency-shifted version. Based on (11), the CAF has peaks at certain cycle frequencies depending on the selection of the employed subcarriers. For example, when only two subcarriers, whose indices are k_1 and k_2, are selected for the transmission of the preamble, the CAF shows a peak only at the cycle frequency $\alpha = \pm(k_1 - k_2)\Delta f$. This is because other subcarriers are not used, that is, $s_{k\notin G}$ is set to zero.

Figure 1 illustrates examples of the frame format. Figure 2 shows examples of the relation between subcarriers used at the inserted preamble and CAF peak pattern for $\nu = 0$, respectively. In both Figures 1 and 2, a 4-subcarrier OFDM signal is used. The preamble part of System A uses the first and third subcarriers, where that for System B uses the first and second subcarriers. Therefore, following (11) and as depicted in Figure 2, a CAF peak for System A is obtained at the cycle frequency of $\alpha = 2\Delta f$, whereas a CAF peak for System B appears at the cycle frequency of $\alpha = \Delta f$. As shown

in this example, the use of different subsets of subcarriers at the preamble part is able to yield CAF peaks at different cycle frequencies.

On the other hand, for the case when the GI is inserted at the preamble, the phase discontinuity at subcarriers caused by the abrupt transition from a symbol to another occurs; therefore, (10) is no longer true, which leads to undesired CAF peaks. From (9), however, we can avoid this phase discontinuity and undesired CAF peaks by selecting the used subcarriers, $k \in G$, such that the following equation is satisfied:

$$e^{j2\pi k\Delta f((\nu+1)N_{\mathrm{dg}}-\nu N_{\mathrm{dg}})T_s} = e^{j2\pi k\Delta f((\nu+1)N_{\mathrm{dg}}-(\nu+1)N_{\mathrm{dg}})T_s}. \quad (12)$$

Obviously, (12) is satisfied if and only if $k\Delta f N_{\mathrm{dg}} T_s$ is an integer. Therefore, we can still make Method A applicable for the case when the GI is inserted at the preamble by selecting the used subcarriers, $k \in G$, such that $k\Delta f N_{\mathrm{dg}} T_s$ is an integer. Such a constraint on the choice of used subcarriers can maintain the phase continuity; however, it reduces the number of CAF peak patterns that can be generated. Therefore, it is preferable not to insert the GI at the preamble part of Method A.

3.2. Method B: Cyclostationarity-inducing transmission method employing dedicated subcarriers at each OFDM symbol

Method B is based on dedicating a few subcarriers at each OFDM symbol to the transmission of specific signals that has the time-domain characteristics configured. In order to induce cyclostationarity, the phase of the signal on the dedicated subcarriers is periodically rotated in the time domain within the OFDM frame. The periodicity of the signal on the dedicated subcarriers is carefully chosen so that the CAF for the whole OFDM frame comprising several OFDM symbols shows peaks at preselected cycle frequencies during data transmission.

The νth transmitted symbols on the dedicated subcarriers are generated as

$$s_{k\in D}[\nu] = e^{j(2\pi\nu/m_k)}, \quad (13)$$

where k is the index of the OFDM subcarrier, D is the set of indices corresponding to the dedicated subcarriers, and m_k is a real number selected such that $0 < 1/m_k < 1$ depending on the system and the dedicated subcarrier. Here, it is also noteworthy that for Method B, the insertion of the GI is mandatory since information symbols are simultaneously transmitted on the remaining subcarriers other than the dedicated subcarriers.

Figures 3 and 4 illustrate examples of the frame format and transmitted symbols on the dedicated subcarriers over one OFDM frame in Method B, respectively. In these figures, it is assumed that the indices of the dedicated subcarriers are 2 and 12 in the OFDM frame, and $m_2 = 8$ and $m_{12} = 7$. In this case, the symbol streams as shown in Figure 4 are transmitted on subcarriers 2 and 12, and information symbols are transmitted on the remaining subcarriers.

Here, the transmitted OFDM-based signal is transformed, using a Fourier series, from (9) to

$$x[i] = \sum_f \left\{ \sum_{k\in D} S_{f,k\in D} + \sum_{k\notin D} S_{f,k\notin D} \right\} e^{j2\pi f i T_s}, \quad (14)$$

where $S_{f,k\in D}$ and $S_{f,k\notin D}$ are the frequency representation of the transmitted signals on the dedicated and data subcarriers, respectively. Here, $S_{f,k\in D}$ is given by

$$S_{f,k\in D} = \frac{1}{\sqrt{V_1 N_{\mathrm{dg}}}} \sum_{i=0}^{V_1 N_{\mathrm{dg}}-1} e^{-j2\pi f i T_s} \times \left[\sum_{\nu=0}^{V_1-1} e^{j(2\pi\nu/m_k)} u\left[\frac{i}{N_{\mathrm{dg}}} - \nu \right] e^{j2\pi k\Delta f(i-\nu N_{\mathrm{dg}})T_s} \right], \quad (15)$$

where V_1 is the number of transmitted OFDM symbols for Method B and $V_1 N_{\mathrm{dg}}$ is the number of samples within the observation interval. Therefore, from (6), the CAF for the OFDM-based signal employing Method B is given by

$$\widetilde{R}_x^{\alpha}[\nu] = \sum_f \left[\sum_{k_1\in D} \sum_{k_2\in D} S_{f,k_1\in D} S^*_{f-\alpha,k_2\in D} e^{-j2\pi(f-\alpha)\nu T_s} \right] + \varepsilon, \quad (16)$$

where ε is the summation of the CAF between the dedicated and data subcarriers, and that between two data subcarriers. Here, assuming that the information symbols transmitted on the data subcarriers are pseudo random, ε converges to zero when $V_1 N_{\mathrm{dg}}$ approaches infinity.

For a sufficiently large V_1, as described in (A.7) in the appendix, the CAF peaks for Method B appear at the cycle frequencies of

$$\alpha = \frac{1/m_{k_1} - 1/m_{k_2} + d'}{N_{\mathrm{dg}} T_s}, \quad (17)$$

where $d' \in \mathbf{Z}$. Especially, the CAF peak with the highest amplitude is obtained for d', which satisfies the following inequality (see the appendix):

$$N_{\mathrm{dg}}(k_1-k_2)\Delta f T_s - \frac{1}{m_{k_1}} + \frac{1}{m_{k_2}} - \frac{1}{2} < d' \le N_{\mathrm{dg}}(k_1-k_2)\Delta f T_s - \frac{1}{m_{k_1}} + \frac{1}{m_{k_2}} + \frac{1}{2}. \quad (18)$$

Therefore, by selecting the values of m_k, we are able to produce CAF peaks at preselected cycle frequencies according to (17), and make the CAF peaks show up at different cycle frequencies for different OFDM-based systems.

The CAF peak patterns, before and after cyclostationarity is being induced using Method B, are illustrated in Figures 5 and 6.

4. SYSTEM RECOGNITION SCHEMES

For the detection process at the receiver, in order to distinguish among secondary systems, the CAFs calculated

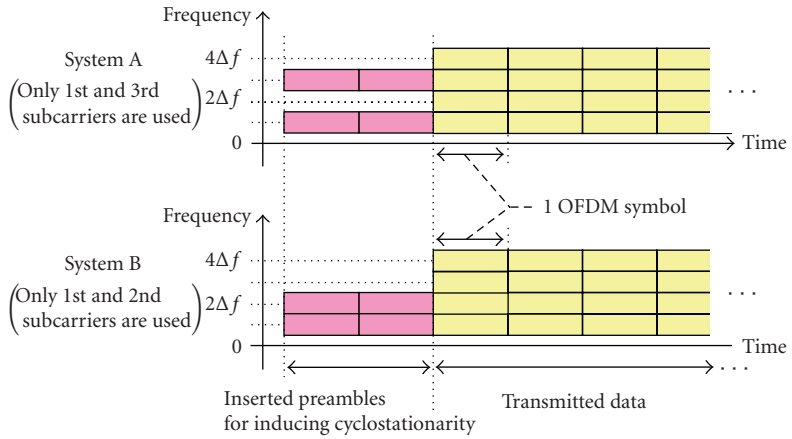

Figure 1: Illustration of frame format for Method A.

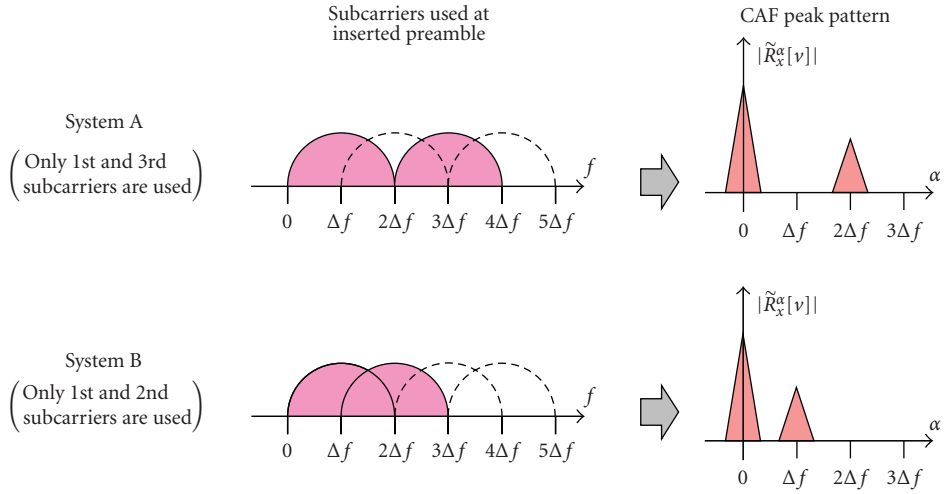

Figure 2: Examples of relation between subcarriers used at inserted preamble and CAF peak pattern ($\nu = 0$) for Method A.

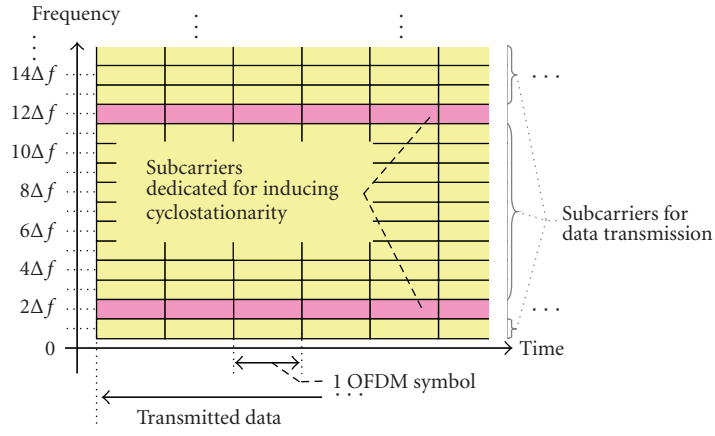

Figure 3: Example of OFDM frame format for Method B.

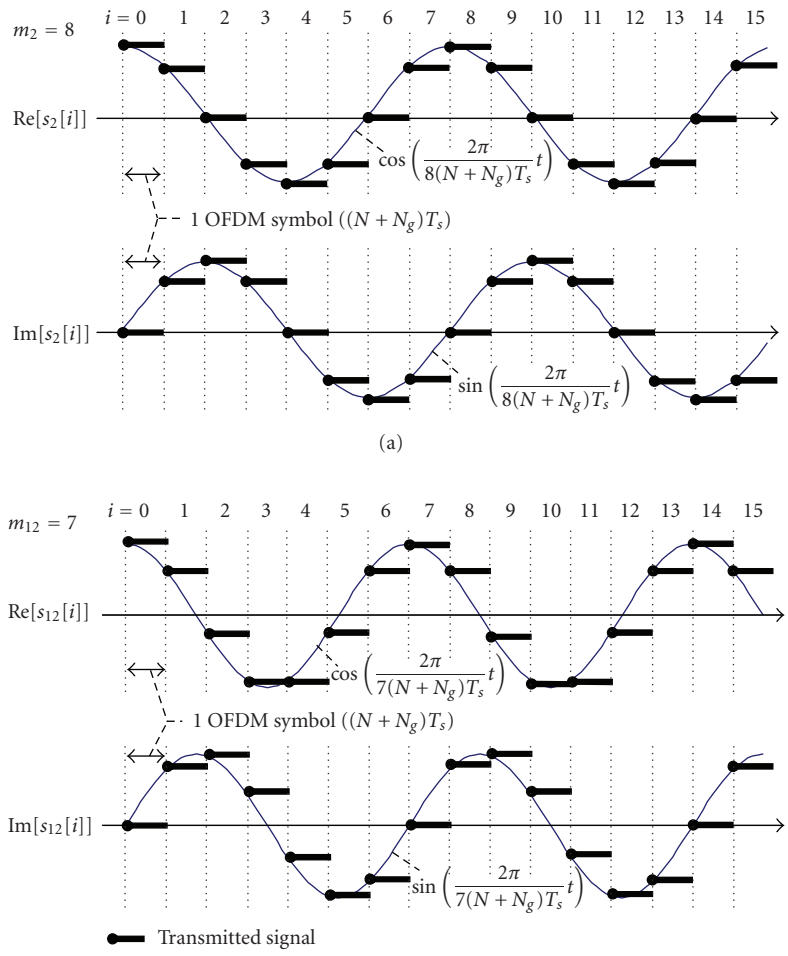

Figure 4: Example of transmitted symbols on dedicated subcarriers.

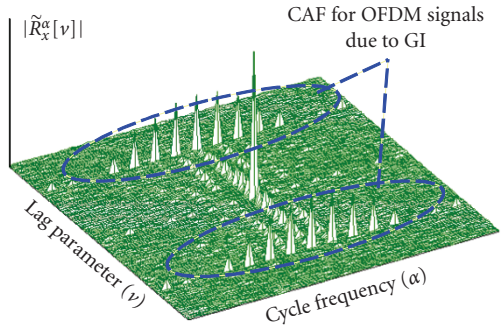

Figure 5: Illustration of CAF peak pattern before cyclostationarity induction.

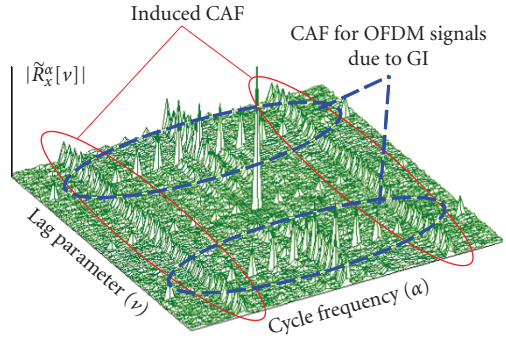

Figure 6: Illustration of CAF peak pattern after cyclostationarity induction using Method B.

from the received signal, $\widetilde{R}_r^{\alpha}[\nu]$, need to be compared with the CAF candidates calculated and stored in advance. Such a comparison basically translates into a multiple hypothesis testing problem between $\mathcal{H}_1, \ldots, \mathcal{H}_Q$, given by [15]

$$\mathcal{H}_q : r[i] = \sum_{\psi=0}^{\Psi} h[\psi] x_q[i-\psi] + n[i], \quad q = 1, \ldots, Q, \tag{19}$$

where $x_q[i]$ is the transmitted signal for system q $(= 1, \ldots, Q$, Q is the number of systems to be distinguished), the channel impulse response, $h[i]$, is assumed to be time-invariant during one OFDM frame, and Ψ is the length of multipath channel. This multiple hypothesis testing problem can be reformulated in terms of CAF as follows [16]:

$$\mathcal{H}_q : \widetilde{R}_r^{\alpha}[\nu] = \widetilde{R}_{x_q,H}^{\alpha}[\nu] + \Delta\widetilde{R}_e^{\alpha}[\nu], \quad q = 1, \ldots, Q, \tag{20}$$

where

$$\widetilde{R}^{\alpha}_{x_q,H}[\nu] = \frac{1}{I_0}\sum_{i=0}^{I_0-1}\left[\sum_{\psi_1=0}^{\Psi-1} x_q[i-\psi_1]h[\psi_1]\right] \times\left[\sum_{\psi_2=0}^{\Psi-1} x_q^*[i+\nu-\psi_2]h^*[\psi_2]\right]\mathrm{e}^{-j2\pi\alpha i T_s} \tag{21}$$

$$= \sum_{\psi_1=0}^{\Psi-1}\sum_{\psi_2=0}^{\Psi-1} h[\psi_1]h^*[\psi_2]\widetilde{R}^{\alpha}_{x_q}[\nu+\psi_1-\psi_2]\mathrm{e}^{-j2\pi\alpha\psi_1 T_s}. \tag{22}$$

Here, $\Delta\widetilde{R}^{\alpha}_{e}[\nu]$ represents the estimation error, which converges to zero asymptotically as the observation interval of the received signal, I_0, approaches infinity when hypothesis $\mathcal{H}_q$ is true. In addition, $\widetilde{R}^{\alpha}_{x_q}[\nu]$ is the CAF for the transmitted signal of the candidate systems. From (22), if α exists such that $\widetilde{R}^{\alpha}_{x_q}[\nu]$ converges to zero regardless of ν, the CAF of the received signal, $\widetilde{R}^{\alpha}_{x_q,H}[\nu]$, also converges to zero.

4.1. Optimum detector

In the maximum likelihood sense, for a certain lag parameter, ν, the optimum detection is performed as [15, 16]

$$q_0 = \arg\max_q \mathrm{Prob}\left(\widetilde{R}^{\alpha}_{r}[\nu] \mid \mathcal{H}_q\right). \tag{23}$$

Assuming that the prior probabilities of transmission for all systems are equal, the minimum distance detector provides optimum detection [15, 16]. The minimum distance detector is performed using the following equation:

$$q_0 = \arg\min_q \sum_{\alpha} \left|\widetilde{R}^{\alpha}_{r}[\nu] - \widetilde{R}^{\alpha}_{x_q,H}[\nu]\right|^2. \tag{24}$$

For the optimum detection, the CAF candidates, $\widetilde{R}^{\alpha}_{x_q,H}[\nu]$, are calculated for every OFDM frame taking into consideration the channel state of the received signal.

In (24), the calculation of the CAF value for every α requires $2I_0$ complex multiplications. For system recognition, the CAF is calculated for multiple cycle frequencies corresponding to every system to be distinguished. If the number of all possible cycle frequencies is A, the number of complex multiplications of CAF calculation for the received signal is $2AI_0$. For the optimum detection, the CAF candidates are calculated taking into consideration the channel impulse response. Here, when the channel is invariant in time during one OFDM frame, we can calculate the CAF candidates using (22). In this case, since the complexity of the calculation of $\widetilde{R}^{\alpha}_{x_q}[\nu]$, which is calculated and stored in advance, can be ignored, the calculation of the CAF candidates at A cycle frequencies for each of Q systems requires $3\Psi^2QA$ complex multiplications. Note that the complexity owing to CSI estimation is not included. In addition, the comparison of the CAFs for the received signal and the transmitted signal for each system requires QA complex multiplications. Therefore, the total number of complex multiplications for the optimum detector is given by $A(2I_0 + (3\Psi^2 + 1)Q))$.

On the other hand, when the channel varies in time, the calculation of CAF candidates cannot utilize the stored $\widetilde{R}^{\alpha}_{x_q}[\nu]$. In this case, therefore, from (21), the calculation of CAF candidates requires $4AQ\Psi I_0$ complex multiplications.

For the detection process, the range of I_0 is given by V_0N and V_1N_{dg} for Methods A and B, respectively. On the other hand, for Method A, A is less than N since the CAF becomes zero at $\alpha \neq n\Delta f$ ($n \in \mathbf{Z}$ and $0 \leq n \leq N-1$). For Method B, from (17), the number of possible cycle frequencies for every system is equal to or less than N_{dg}. Therefore, for Method B, A is equal to or less than QN_{dg}.

For the optimum detector, however, the CSI of the received signals is required to calculate the CAF candidates. In addition, since the phase of $\widetilde{R}^{\alpha}_{x_q}[\nu]$ is dependent on the center frequency of the received signal and the observation interval, the knowledge of the center frequency and the start and end timings of the observation interval are required. Nevertheless, the assumption of a known channel is not practical, and therefore the optimum detector may not be realistically applicable.

4.2. Suboptimum detector

We introduce here a suboptimum detector that does not require CSI. This suboptimum detector simply detects whether or not the CAF for the received signal shows peaks, that is, energy in the possible CAF patterns corresponding to the candidate systems. This can be carried out by comparing the amplitudes of the CAF for the received signal, $|\widetilde{R}^{\alpha}_{r}[\nu]|$, with those of the CAF for the transmitted signal of the candidate systems, $|\widetilde{R}^{\alpha}_{x_q}[\nu]|$ ($q = 1, 2, \ldots$), for all possible cycle frequencies as expressed in the following equation:

$$q_0 = \arg\min_q \sum_{\alpha} \left(|\widetilde{R}^{\alpha}_{r}[\nu]| - |\widetilde{R}^{\alpha}_{x_q}[\nu]|\right)^2. \tag{25}$$

Therefore, in this suboptimum detector, the amplitudes of $\widetilde{R}^{\alpha}_{x_q}[\nu]$ serve as CAF candidates. In this suboptimum detection, no knowledge of center frequency is required. In fact, from (2), the CAF for the signal $r_0[i] = r[i]\mathrm{e}^{j2\pi f_c i T_s}$, where f_c is the center frequency, is given by

$$\widetilde{R}^{\alpha}_{r_0}[\nu] = \sum_{i=0}^{I_0-1}\left\{r[i]\mathrm{e}^{j2\pi f_c i T_s}\right\}\left\{r^*[i+\nu]\mathrm{e}^{-j2\pi f_c (i+\nu)T_s}\right\}\mathrm{e}^{-j2\pi\alpha i T_s} = \widetilde{R}^{\alpha}_{r}[\nu]\mathrm{e}^{-j2\pi f_c \nu T_s}. \tag{26}$$

From (26), we obtain $|\widetilde{R}^{\alpha}_{r_0}[\nu]| = |\widetilde{R}^{\alpha}_{r}[\nu]|$, and therefore, we can use $|\widetilde{R}^{\alpha}_{r_0}[\nu]|$ instead of $|\widetilde{R}^{\alpha}_{r}[\nu]|$ in (25). Besides, for the suboptimum detector, coarse timing synchronization is sufficient as no CSI is required.

In (25), these CAF candidates are normalized such that for each system the total power distributed on the CAF peaks is equal. Under this condition, the use of our suboptimum detector is also equivalent to the use of a crosscorrelation

detector among the amplitudes of CAF peaks calculated from the received signal and CAF candidates. More specifically, (25) can be rewritten as

$$q_0 = \arg\max_q \sum_\alpha \left|\widetilde{R}^{\alpha}_{r}[\nu]\right| \left|\widetilde{R}^{\alpha}_{x_q}[\nu]\right|. \tag{27}$$

To understand how this suboptimum detector works, let us look at the case when the CAF for system q has a peak only at $\alpha = \alpha_q$ for at least one lag parameter, ν, that is, $\widetilde{R}^{\alpha}_{x_q}[\nu]$ becomes zero at $\alpha \neq \alpha_q$. For this case, when the received signal belongs to system q', the summation in (27) can be expressed, using (22), as

$$\begin{aligned}
&\sum_\alpha \left|\widetilde{R}^{\alpha}_{r}[\nu]\right| \left|\widetilde{R}^{\alpha}_{x_q}[\nu]\right| \\
&\quad = \left|\widetilde{R}^{\alpha_q}_{r}[\nu]\right| \left|\widetilde{R}^{\alpha_q}_{x_q}[\nu]\right| \\
&\quad = \left| \sum_{\psi_1=0}^{\Psi-1} \sum_{\psi_2=0}^{\Psi-1} h[\psi_1] h^*[\psi_2] \widetilde{R}^{\alpha_q}_{x_{q'}}[\nu+\psi_1-\psi_2] \mathrm{e}^{-j2\pi\alpha_q\psi_1 T_s} \right. \\
&\qquad \left. + \Delta\widetilde{R}^{\alpha_q}_{e}[\nu] \right| \left|\widetilde{R}^{\alpha_q}_{x_q}[\nu]\right|.
\end{aligned} \tag{28}$$

Here, for $q \neq q'$, $\widetilde{R}^{\alpha_q}_{x_{q'}}[\nu]$ is zero; the crosscorrelation of (28) becomes $|\Delta\widetilde{R}^{\alpha_q}_{e}[\nu]||\widetilde{R}^{\alpha}_{x_q}[\nu]|$, which converges to a negligibly small value compared to that for $q = q'$ when the observation interval becomes sufficiently large. As a result, this suboptimum detector is able to recognize the system to which the received signal belongs without requiring the CSI. In this regard, for a general case, however, the signals need to be configured so that $\widetilde{R}^{\alpha_q}_{x_{q'}}[\nu]$ approaches zero for each pair of two systems q and q'.

In Method B, for example, the CAF is given by (A.6). When system q' has a cycle frequency of $\alpha_{q'} = (1/m'_{k_1} - 1/m'_{k_2} + d'_{q'})/N_{\mathrm{dg}}T_s$, whereas the CAF is calculated for system q, $\alpha_q = (1/m_{k_1} - 1/m_{k_2} + d'_q)/N_{\mathrm{dg}}T_s$, according to (A.6) the first summation of the right-hand side of the CAF, $\widetilde{R}^{\alpha_q}_{x_{q'}}[\nu]$, can be rewritten as

$$\begin{aligned}
&\sum_{\nu=0}^{V_1-1} \mathrm{e}^{j2\pi\nu\{1/m'_{k_1} - 1/m'_{k_2} - \alpha_q N_{\mathrm{dg}} T_s\}} \\
&\qquad = \frac{1 - \mathrm{e}^{-j2\pi V_1\{1/m'_{k_1} - 1/m'_{k_2} - \alpha_q N_{\mathrm{dg}} T_s\}}}{1 - \mathrm{e}^{j2\pi\{1/m'_{k_1} - 1/m'_{k_2} - \alpha_q N_{\mathrm{dg}} T_s\}}}.
\end{aligned} \tag{29}$$

Therefore, according to (29), in order to reduce $\widetilde{R}^{\alpha_q}_{x_{q'}}[\nu]$ to zero, $\{m_{k_1}, m_{k_2}\}$ and $\{m'_{k_1}, m'_{k_2}\}$ corresponding to every pair of systems are to be selected so that $V_1(1/m'_{k_1} - 1/m'_{k_2} - (1/m_{k_1} - 1/m_{k_2}))$ is as close as possible to a nonzero integer. For example, when it is possible to select values of m_k from divisors of the number of transmitted OFDM symbols, V_1, $\widetilde{R}^{\alpha_q}_{x_{q'}}[\nu]$ can be reduced to zero.

Regarding the complexity for the suboptimum detector, since no CSI is used for the calculation of CAF candidates, the number of the complex multiplications needed is reduced compared to the optimum detection to $A(2I_0 + Q)$.

4.3. Extended detectors

Since the above suboptimum detector detects only whether or not the CAF is present at a preselected cycle frequency, this detector corresponds to an energy detector in the CAF domain [17]. Similarly, the above optimum detector corresponds to a matched filter detector in the CAF domain. Therefore, in order to achieve comparable detection probability, the suboptimum detector inherently requires an observation interval, I_0, longer than that for the optimum detector [9, 18]. To enhance the detection performance without expanding I_0, we harness the fact that the induced CAF for the proposed cyclostationarity-inducing methods (cf. Figure 6) has peaks over multiple lag parameters, ν, and extend the suboptimum detector such that it utilizes the CAF peaks over L lag parameters, ν_l ($l = 0, 1, \ldots, L-1$). By using L lag parameters, the number of samples that can be used is increased and simultaneously the number of diversity branches that can be utilized against channel fading also becomes larger.

The extended suboptimum detector corresponding to (25) is then performed as

$$q_0 = \arg\min_q \sum_\alpha \sum_{l=0}^{L-1} \left(\left|\widetilde{R}^{\alpha}_{r}[\nu_l]\right| - \left|\widetilde{R}^{\alpha}_{x_q}[\nu_l]\right| \right)^2. \tag{30}$$

According to (30), since the extended detector calculates and compares the CAFs for L lag parameters, the total number of complex multiplications for the extended detector is given by $LA(2I_0 + Q)$.

We should note here that the extended detector can also be applied to the optimum detector in a similar manner as indicated above.

5. COMPUTER SIMULATION

Using computer simulation, the detection probabilities when using the proposed methods to induce cyclostationarity at the transmitter are evaluated when the optimum and suboptimum detectors are used to recognize the system to which the received signal, $r[i] = r(iT_s)$, belongs. The number of OFDM-based systems to be distinguished is assumed to be 4, where only one transmitter of the four systems is allowed to transmit during each OFDM frame. The simulation parameters are shown in Table 1, and the system model is shown in Figure 7.

Performance evaluations are conducted for both AWGN and multipath Rayleigh fading channels. The multipath Rayleigh fading channel model used is shown in Figure 8.

5.1. Parameter settings for proposed methods

In the following, performance evaluations are performed when the number of nonzero subcarriers used at the preamble in Method A, $|G|$, and the number of dedicated subcarriers in Method B, $|D|$, are both equal to 6. Here, $|\cdot|$ denotes the cardinality of a set. Obviously, for Methods A and B, an increase in the number of subcarriers used, even under a constant sum power constraint, improves the detection

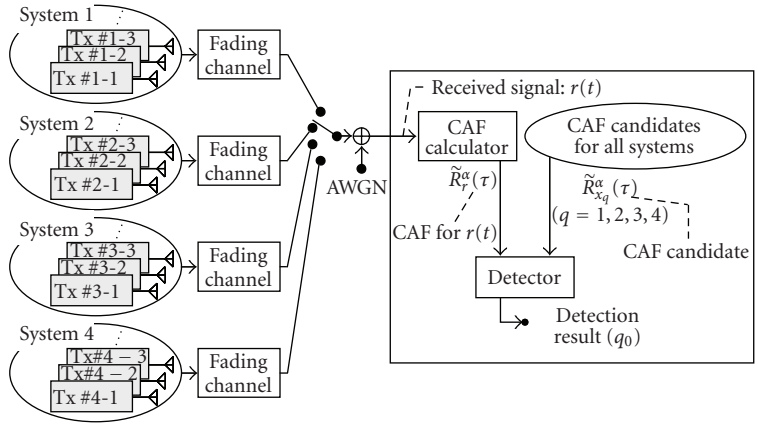

Figure 7: System model.

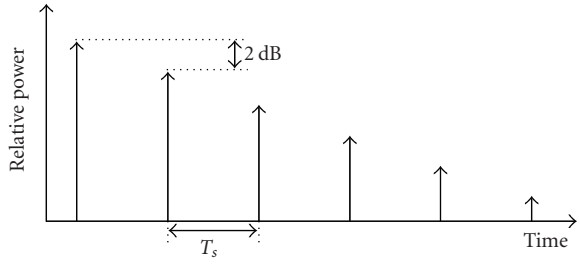

Figure 8: Channel model.

Table 1: Simulation parameters.

	Method A	Method B
No. of systems to be distinguished	4	
FFT length	64	
GI length	0	16
No. of subcarriers used for signal recognition	6 (Used subcarriers at preamble)	6 (Dedicated subcarriers)
No. of symbols used for system recognition	$V_0 = 2$ symbols	$V_1 = 64$ symbols
Channel model	Exponentially decayed 6-path Rayleigh fading channel (Max. Doppler freq., $f_D \simeq 0$ Hz)	

probability over frequency-selective fading. However, this comes at the price of a decrease in the number of systems that can be distinguished in Method A and the number of subcarriers that can be used for data transmission in Method B.

Since only a limited number of subcarriers are used for Methods A and B, the employed subcarriers need to be arranged carefully so that the diversity gain against frequency-selective fading can be obtained. Meanwhile, the subset of subcarriers used in Method A and parameter m_k for Method B need to be carefully set so that $\widetilde{R}^{\alpha_q}_{x_{q'}}[\nu]$ approaches zero for $q \neq q'$. Thereby, the detection probability of the optimum and suboptimum detectors is improved.

In order to satisfy the above-mentioned requirements, for Method A, having a DFT size of 64, the subcarriers used for preamble transmission are selected as follows.

(1) The indices of used subcarrier, k, are selected from less than 32, and the kth used subcarrier are copied into the $(k + 32)$th subcarrier.

(2) CAFs for every two systems do not show peaks at the same cycle frequency.

Table 2 shows the indices of the selected subcarriers for Method A.

On the other hand, for Method B, the set of indices is fixed to $D = \{7, 17, 27, 39, 49, 59\}$ and the values for m_k are shown in Table 3. The values of m_k are selected so that the following conditions hold.

Table 2: Indices of selected subcarriers and their corresponding cycle frequencies in Method A.

$\lvert G\rvert = 6$	G	Cycle frequency at which CAF has peaks ($\times\Delta f$)
System 1	1, 3 , 7, 33, 35, 39	2, 4, 6, 26, 28, 30
System 2	1, 4, 13, 33, 36, 45	3, 9, 12, 20, 23, 29
System 3	1, 6, 16, 33, 38, 48	5, 10, 15, 17, 22, 27
System 4	1, 9, 20, 33, 41, 52	8, 11, 13, 19, 21, 24

Table 3: Values for m_k in (13).

	m_7, m_{17}, m_{27}	m_{39}, m_{49}, m_{59}	Cycle frequency at which CAF has peaks ($\times 1/N_{\mathrm{dg}}T_s$)
System 1	2	4	$1/4 + d'$
System 2		8	$3/8 + d'$
System 3		16	$7/16 + d'$
System 4		32	$15/32 + d'$
			$d' = 15, 27, 40, 52, 65$

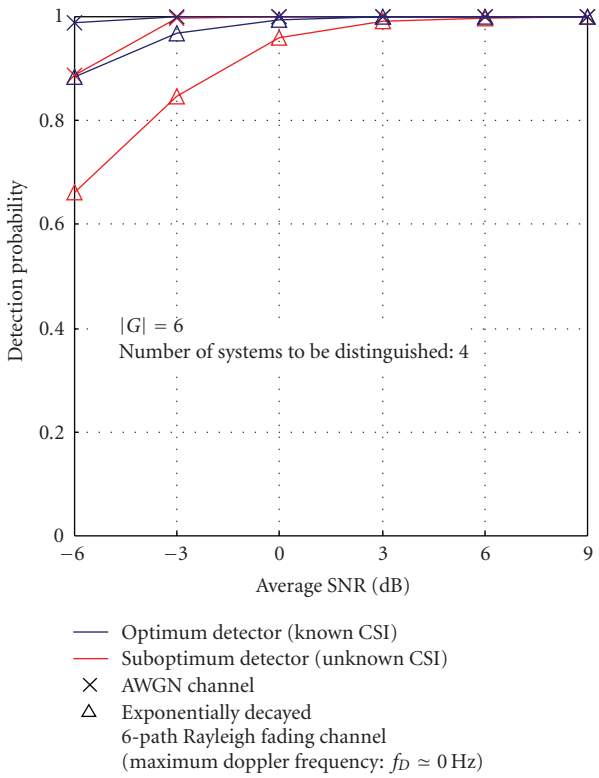

Figure 9: Performance for Method A: optimum and suboptimum detection.

(1) The following pairs of the dedicated subcarriers, three pairs $[\{7,39\},\{17,49\},\{27,59\}]$, two pairs $[\{7,49\},\{17,59\}]$, and two pairs $[\{17,39\},\{27,49\}]$, generate a CAF peak at the same cycle frequency, respectively.

(2) All values of m_k are divisors of the number of transmitted OFDM symbols in one frame, $V_1 = 64$.

Signal recognition is performed by calculating the CAF at multiple cycle frequencies for every system. For example, the CAF is calculated at all the cycle frequencies in Table 2 for Method A, and in Table 3 for Method B, when d' in (17) is set to $\{15, 27, 40, 52, 65\}$.

5.2. Detection performance for Method A

In the following simulations, the CAF used is calculated for a lag parameter of $\nu = 0$. In addition, the CAF calculation is performed using $I_0 = V_0 N = 128$ samples, that is, $V_0 = 2$ symbols.

5.2.1. Optimum detector

Figure 9 shows the detection performance using the optimum detector, which is given in (24) for AWGN and multipath Rayleigh fading channels. Simulation results show that Method A enables the receiver to distinguish among multiple OFDM-based systems even when their natural cyclostationarity properties are the same. This confirms that Method A properly induces artificial cyclostationarity. Indeed, in Figure 9, using the optimum detector, the detection probability of 99% is achieved in the SNR range of greater than -3 dB for the AWGN channel.

On the contrary, the detection performance is degraded for the frequency-selective channel compared to the AWGN channel. This is because the frequency selectivity of the channel causes a decrease in the number of CAF peaks that can be utilized at the detector.

5.2.2. Suboptimum detector

The use of the suboptimum detector, which is given in (25), also leads to degradation of the detection performance in Figure 9. This is because the optimum detector can utilize its knowledge of CSI to enhance the desired CAF peaks and suppress the undesired ones. Whereas the suboptimum detector starts by norm computation to align the phases of all CAF peaks to zero, which yields its incapability of suppressing undesired CAF peaks and, therefore, degradation of its detection performance.

Nevertheless, even when the suboptimum detector is used, the detection probability obtained is still acceptable. In fact, the suboptimum detector attains the detection probability of 99% for the SNR range of greater than 3 dB.

5.3. Detection performance for Method B

In the following simulations, the observation interval of the CAF calculation is set to the length of the OFDM frame, that is, the observation interval, I_0, is $N_{\mathrm{dg}} V_1 = 5120$ samples. The detection probability is evaluated for the cases when using the extended versions of the optimum and suboptimum detectors, which were introduced in Section 4. For Method B, the undesired CAF peaks generated by the data subcarriers severely interfere with the CAF peaks generated by the dedicated subcarriers. The use of the extended detectors allow for better averaging of this interference as the number of samples used increases linearly with the number of lag parameters, L. Also in these simulations, the lag parameters employed for the detection in (30), ν_l, are set to $2l$ [sample], $(l = 0, 1, 2, \ldots, L-1)$.

5.3.1. Optimum detector

Figure 10 shows the detection performance for AWGN and multipath Rayleigh fading channels. In these simulations, it is assumed that $L = 5$. These simulation results show that Method B also enables cyclostationarity-based signal recognition among multiple OFDM-based systems.

5.3.2. Suboptimum detector

When the suboptimum detector is used, the detection performance for Method B is also degraded. However, good detection performance is maintained and 99% of detection probability can be achieved in the SNR range of greater than 6 dB for multipath Rayleigh fading channel.

5.3.3. *Extended detectors with $L = 1, 5$ and 10 under multipath Rayleigh fading conditions*

Figure 11 shows the detection probability for Method B when the extended optimum and suboptimum detectors with $L = 1$, 5, and 10 in (30) are used in the multipath Rayleigh fading channel. Note that, with $L = 1$, the extended optimum and suboptimum detectors are just the optimum and suboptimum detector. As shown in Figure 11, with $L = 1$, the detection probability is degraded compared to that for Method A. This is because, for Method B, undesired CAF peaks occur due to not only noise but also data subcarriers. In addition, for the multipath Rayleigh fading channel, desired CAF peaks are suppressed due to the frequency-selectivity of the channel, while undesired CAF peaks owing to data subcarriers remain since the number of data subcarriers is larger than that of the dedicated subcarriers. On the other hand, the simulation results show that the detection performance can indeed be effectively improved by increasing L. Especially, a detection probability that is larger than 99% is attained in the SNR range of more than 3 dB when the extended suboptimum detector with $L = 10$ is used.

5.4. *Detection performance for Methods A and B using suboptimum detector under fast fading conditions*

In order to examine the impact of fast channel fluctuations on the detection performance of Methods A and B, the detection probability is evaluated as a function of the Doppler frequency. The simulation results are shown in Figure 12. For Method A, the suboptimum detector is used for the evaluation of the detection probability, meanwhile the extended suboptimum detector, with $L = 10$, is used for Method B. In addition, the evaluation is performed for the average SNR = 6 dB.

Figure 12 shows that the signal recognition based on Method A achieves good detection performance irrespective of the Doppler frequency, f_D. In contrast, it is shown that the detection probability for Method B is degraded when the Doppler frequency increases. Nevertheless, the practical range of the normalized Doppler frequency is sufficiently low. For example, if we employ the 802.11a format, 4.0×10^{-3} of the normalized Doppler frequency is equal to 1250 Hz of the actual Doppler frequency, and this corresponds to a moving speed of approximately 270 km/h. Therefore, these simulation results show that signal recognition based on both proposed methods can maintain good detection performance within the range of practical Doppler frequencies.

6. DISCUSSION

As revealed in the simulation results, by employing the proposed methods, cyclostationarity can be induced and multiple OFDM-based systems can be distinguished. However, the proposed methods have their own advantages and drawbacks.

One common important issue is that of the additional overhead incurred by both methods. For Method A, the

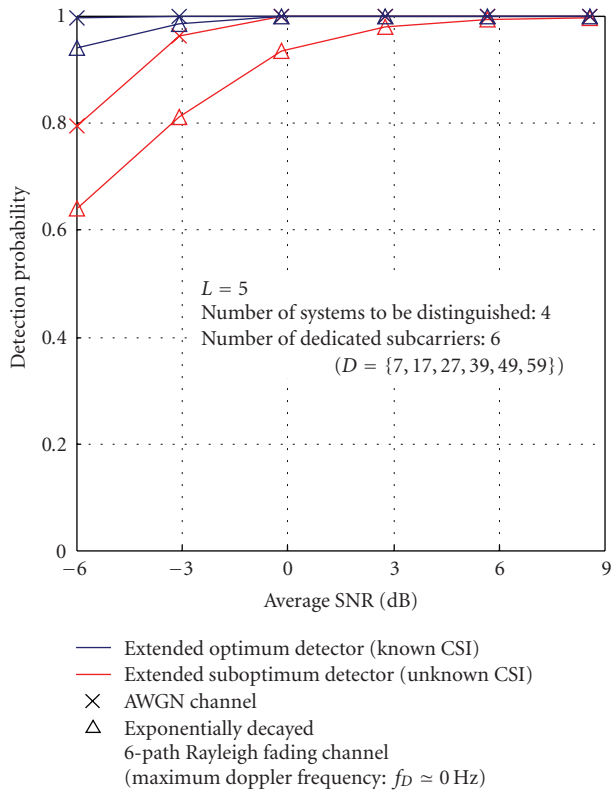

Figure 10: Performance for Method B: extended optimum and suboptimum detection with $L = 5$.

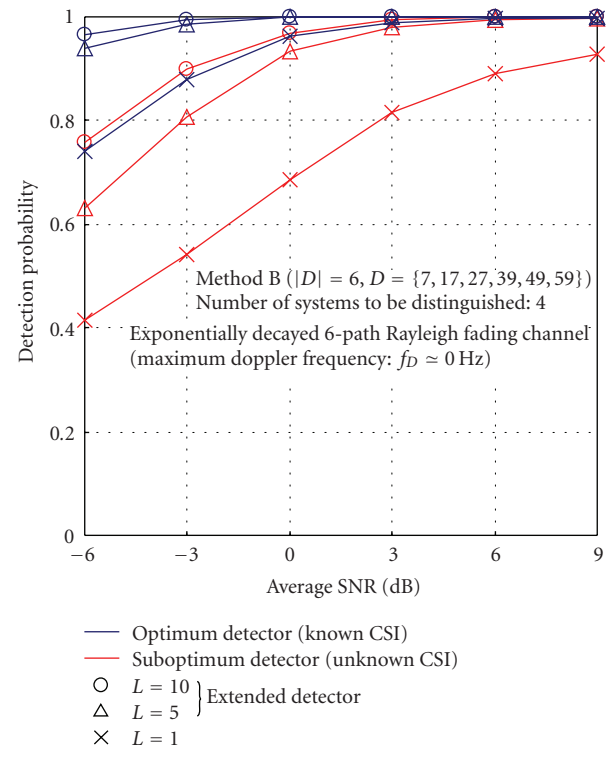

Figure 11: Performance for Method B: extended optimum and suboptimum detection with $L = 1, 5$ and 10.

amount of overhead is V_0KN because no data symbols can be transmitted during the preamble part and therefore all K subcarriers are occupied for the preamble transmission. In addition, when the number of the OFDM symbols per frame is Γ, the percentage of overhead out of every OFDM frame becomes $V_0/\Gamma \times 100\%$. On the other hand, for Method B, the amount of overhead is $|D|N_{\mathrm{dg}}V_1$, where $|D|$ and V_1 are the numbers of dedicated subcarriers and transmitted OFDM symbols, respectively. The percentage of the overhead out of every OFDM frame becomes $|D|/K \times 100\%$.

The amount of overhead is nonnegligible even when a few symbols are employed for the preamble and dedicated subcarriers. For Method A, during the specific preamble transmission, no data can be transmitted. For Method B, the increase in the number of dedicated subcarriers leads to a decrease in the number of data subcarriers in addition to an increase in the power allocated to the dedicated subcarriers. To reduce the amount of overhead, some solutions are considered. One potential candidate is to make the preamble and dedicated subcarriers serve for additional functionalities. For example, the pilot subcarriers, which are widely and mainly used for frequency offset and phase noise compensation in OFDM-based standards such as DVB-T [19] and 802.11a, could also be used as dedicated subcarriers for Method B.

Regarding the detection performance, for Methods A and B, the detection probability can be basically improved by increasing the overhead. In fact, the minimum number of samples required for the cyclostationarity detection so that the signals become detectable is $O((\mathrm{SNR})^{-2})$ samples [9]. In addition, when the same amount of overhead is incurred, the detection performance for Methods A and B is expected to become nearly equal. For example, let us see the case when an equal overhead is paid for Methods A and B. For this case, the detection performance is evaluated based on computer simulation in Figure 13 for Methods A and B when using the optimum detector. In the simulations, it is assumed that the number of subcarriers used for the preamble and that of the dedicated subcarriers are the same, and no data symbols are transmitted for Method B, that is, $|G| = |D| = K$. In addition, we assume that Method A has no GI while Method B includes GI, $N = 64$ and $N_{\mathrm{dg}} = 80$; and therefore, in order to satisfy the equal overhead condition, that is, $V_1KN = |D|N_{\mathrm{dg}}V_1$, the numbers of the OFDM symbols for Methods A and B are set to $V_0 = 80$ and $V_1 = 64$, respectively.

As can be confirmed in Figure 13, the detection probability becomes nearly equal for both methods. However, the performance for Method B is slightly degraded compared to that for Method A. This is because the highest amplitude of the CAF for Method B is less than that for Method A. In fact, from (A.8), in the case when the amplitude of the transmitted signal is 1, that is, $|s_k[i]| = 1$, the highest amplitude of the CAF for Method B becomes less than or equal to 1, while from (11), the CAF peak for Method A has the amplitude of 1 in that case. From (A.8), the highest amplitude of the CAF for Method B becomes 1 if and only if

$$(k_1 - k_2)\Delta f N_{\mathrm{dg}} T_s - \frac{1}{m_{k_1}} + \frac{1}{m_{k_2}} - d' = 0. \qquad (31)$$

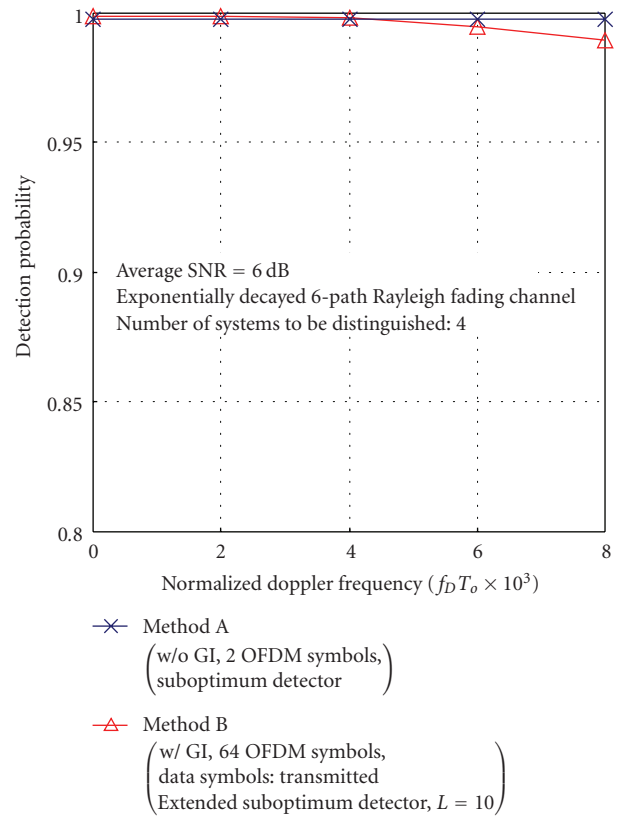

Figure 12: Performance for Methods A and B as a function of Doppler frequency.

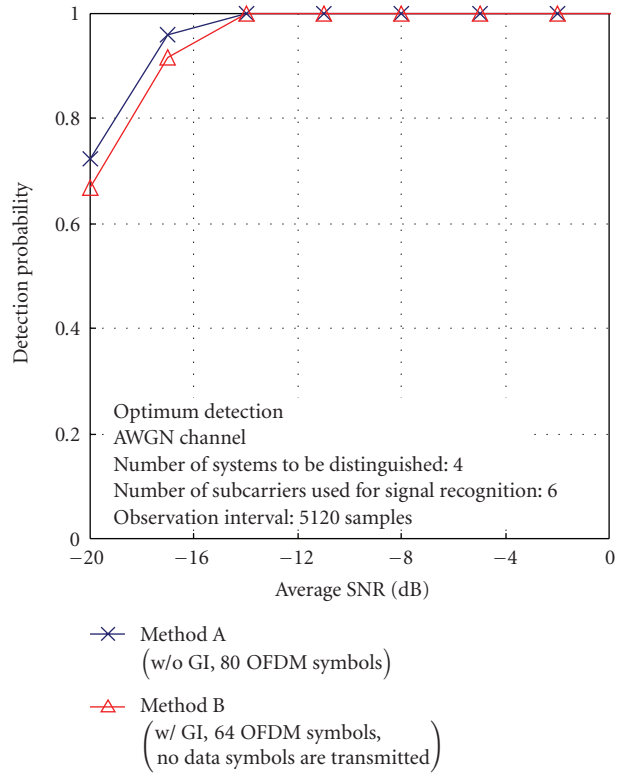

Figure 13: Comparison of detection performance of Methods A and B for the same amount of overhead.

However, since it is restrictive to set m_k so that all pairs of values of m_k satisfy (31), the highest amplitude of the CAF for Method B is lower than that for Method A; therefore, the detection probability for Method B is inherently slightly inferior to that for Method A. However, Method B has the advantage that cyclostationarity can still be induced even when the positions of the usable subcarriers for inducing cyclostationarity are fixed. In addition, Method B is applicable even with the GI while it is preferable not to insert the GI for Method A.

7. CONCLUSION

In this paper, we proposed two configuration methods for the OFDM signal before transmission such that its cyclic autocorrelation function (CAF) is nonzero at certain preselected cycle frequencies. The first proposed method is based on inserting a specific preamble at the beginning of an OFDM frame. The second proposed method is based on dedicating several subcarriers. Using both proposed methods, we are able to induce artificially cyclostationarity in OFDM signals even when a common OFDM-based air interface is used. Using computer simulation, both proposed methods are evaluated under AWGN and multipath Rayleigh fading conditions when the optimum, suboptimum, and extended suboptimum detectors are used at the receiver. The simulation results show that the detection probability for both proposed methods is sufficiently good when the optimum detector is employed. The detection performance for the suboptimum detector is also still acceptable and can be improved using the extended suboptimum detector. Discussions on robustness against the Doppler effect and overhead reveal the advantages and disadvantages of both methods.

As future work, one important issue is to improve the detection probability of proposed cyclostationarity-inducing transmission methods for practical detectors and under the constraint of a minimal amount of overhead.

APPENDIX

In this appendix, we derive the CAF peaks induced by Method B. It is shown that these CAF peaks appear at the cycle frequencies of (17).

For Method B, from (15), the frequency representation of the transmitted signal on dedicated subcarrier $k \in D$ is given by

$$S_{f,k\in D} = \frac{1}{\sqrt{V_1 N_{\mathrm{dg}}}}\left[\sum_{\nu=0}^{V_1-1} \mathrm{e}^{j2\pi\nu\{1/m_k - fN_{\mathrm{dg}}T_s\}}\right] \times \left[\sum_{i_0=0}^{N_{\mathrm{dg}}-1} \mathrm{e}^{-j2\pi(f-k\Delta f)i_0 T_s}\right]. \tag{A.1}$$

Therefore, from (16), assuming $\varepsilon = 0$, when the signal contains only two dedicated subcarriers of indices k_1 and k_2, the CAF is given by

$$\begin{aligned}\widetilde{R}_x^{\alpha}[\nu] &= \sum_f S_{f,k_1\in D} S^*_{f-\alpha,k_2\in D} \mathrm{e}^{-j2\pi(f-\alpha)\nu} \\ &= \frac{1}{V_1 N_{\mathrm{dg}}} \sum_{\nu_1=0}^{V_1-1}\sum_{\nu_2=0}^{V_1-1}\sum_{i_1=0}^{N_{\mathrm{dg}}-1}\sum_{i_2=0}^{N_{\mathrm{dg}}-1}\left[\sum_f \{\mathrm{e}^{-j2\pi f((\nu_1-\nu_2)N_{\mathrm{dg}}+i_1-i_2+\nu)T_s}\} \times \mathrm{e}^{j2\pi\{\nu_1/m_{k_1}-\nu_2/m_{k_2}-\alpha\nu_2 N_{\mathrm{dg}}T_s\}} \times \mathrm{e}^{j2\pi\{-k_1\Delta f i_1 T_s + k_2\Delta f i_2 T_s - \alpha i_2 T_s + \alpha\nu T_s\}}\right].\end{aligned} \tag{A.2}$$

Equation (A.2) becomes zero except when

$$(\nu_1-\nu_2)N_{\mathrm{dg}} + i_1 - i_2 + \nu = 0. \tag{A.3}$$

By writing the variable ν as $\mu N_{\mathrm{dg}} + \eta$, where $\mu \geq 0$, $0 \leq \eta < N_{\mathrm{dg}}$, and $\mu, \eta \in \mathbf{Z}$, (A.3) can be rewritten as

$$(\nu_1-\nu_2+\mu)N_{\mathrm{dg}} + i_1 - i_2 + \eta = 0. \tag{A.4}$$

Since $0 \leq i_1, i_2, \eta \leq N_{\mathrm{dg}} - 1$, (A.4) is satisfied if and only if

$$\begin{aligned} &i_1 - i_2 + \eta = 0 \text{ or } N_{\mathrm{dg}}, \\ &\nu_1 - \nu_2 + \mu = \begin{cases} 0, & i_1 - i_2 + \eta = 0, \\ 1, & i_1 - i_2 + \eta = N_{\mathrm{dg}}. \end{cases}\end{aligned} \tag{A.5}$$

For the case when $i_1 - i_2 + \eta = 0$, by substituting (A.5) into (A.2),

$$\begin{aligned}\widetilde{R}_x^{\alpha}[\nu] = \frac{1}{V_1 N_{\mathrm{dg}}} &\mathrm{e}^{j2\pi\{\mu/m_{k_2} - \eta k_2 \Delta f T_s\}} \\ &\times \sum_{\nu_2=0}^{V_1-1} \mathrm{e}^{j2\pi(\nu_2-\mu)\{1/m_{k_1}-1/m_{k_2}-\alpha N_{\mathrm{dg}}T_s\}} \\ &\times \sum_{i_2=0}^{N_{\mathrm{dg}}-1} \mathrm{e}^{-j2\pi(i_2-\eta)\{(k_1-k_2)\Delta f-\alpha\}T_s}.\end{aligned} \tag{A.6}$$

From the first summation of the right-hand side of (A.6), the CAF has peaks at the cycle frequencies of

$$\alpha = \frac{1/m_{k_1} - 1/m_{k_2} + d'}{N_{\mathrm{dg}} T_s}, \tag{A.7}$$

where $d' \in \mathbf{Z}$. In addition, the CAF amplitude at other cycle frequencies becomes negligibly small compared to that for (A.7) for sufficiently large V_1. On the other hand, using (A.6) and (A.7), the amplitude of the CAF at the cycle frequencies of (A.7) is given by

$$\begin{aligned}&\frac{1}{N_{\mathrm{dg}}}\left|\sum_{i_2=0}^{N_{\mathrm{dg}}-1} \mathrm{e}^{-j2\pi i_2\{(k_1-k_2)\Delta f-(1/m_{k_1}-1/m_{k_2}+d')/N_{\mathrm{dg}}\}T_s}\right| \\ &\quad = \frac{1}{N_{\mathrm{dg}}}\left|\frac{1-\mathrm{e}^{-j2\pi\{N_{\mathrm{dg}}(k_1-k_2)\Delta f T_s - 1/m_{k_1}+1/m_{k_2}-d'\}}}{1-\mathrm{e}^{-j2\pi\{(k_1-k_2)\Delta f T_s-(1/m_{k_1}-1/m_{k_2}+d')/N_{\mathrm{dg}})\}}}\right|.\end{aligned} \tag{A.8}$$

In (A.8), since d' is an integer, only the denominator is a function of d'; therefore, the amplitude of the CAF has the largest value for integer d' nearest to $N_{\mathrm{dg}}(k_1 - k_2)\Delta f T_s - 1/m_{k_1} + 1/m_{k_2} + d'' N_{\mathrm{dg}}$, where $d'' \in \mathbf{Z}$. Here, from (2), the CAFs for $\alpha = \alpha_0$ and $\alpha = \alpha_0 + a/T_s$ ($a \in \mathbf{Z}$) are equivalent. Therefore, from (A.7), the CAFs for $d' = d_0$ and $d' = d_0 + d_1 N_{\mathrm{dg}}$, ($d_0, d_1 \in \mathbf{Z}$), are also equivalent. As a result, we can simply focus on the case when $d'' = 0$. Accordingly, d' which gives the maximum amplitude of the CAF is given as the integer satisfying the following inequality:

$$N_{\mathrm{dg}}(k_1 - k_2)\Delta f T_s - \frac{1}{m_{k_1}} + \frac{1}{m_{k_2}} - \frac{1}{2} < d' \leq N_{\mathrm{dg}}(k_1 - k_2)\Delta f T_s - \frac{1}{m_{k_1}} + \frac{1}{m_{k_2}} + \frac{1}{2}. \tag{A.9}$$

For the case when $i_1 - i_2 + \eta = N_{\mathrm{dg}}$, we can easily show that, in a manner similar to the case when $i_1 - i_2 + \eta = 0$, the same results as those for (A.7) and (A.9) are obtained.

ACKNOWLEDGMENT

This paper was presented in part at the IEEE Symposium on New Frontiers in Dynamic Spectrum Access Networks (DySPAN 2007) in April 2007.

REFERENCES

[1] T. A. Weiss and F. K. Jondral, "Spectrum pooling: an innovative strategy for the enhancement of spectrum efficiency," *IEEE Communications Magazine*, vol. 42, no. 3, pp. S8–S14, 2004.

[2] M. Öner and F. K. Jondral, "On the extraction of the channel allocation information in spectrum pooling systems," *IEEE Journal on Selected Areas in Communications*, vol. 25, no. 3, pp. 558–565, 2007.

[3] C. Cordeiro, K. Challapali, D. Birru, and N. S. Shankar, "IEEE 802.22: the first worldwide wireless standard based on cognitive radios," in *Proceedings of the 1st IEEE International Symposium on New Frontiers in Dynamic Spectrum Access Networks (DySPAN '05)*, pp. 328–337, Baltimore, Md, USA, November 2005.

[4] J. Mitola III and G. Q. Maguire Jr., "Cognitive radio: making software radios more personal," *IEEE Personal Communications*, vol. 6, no. 4, pp. 13–18, 1999.

[5] S. Haykin, "Cognitive radio: brain-empowered wireless communications," *IEEE Journal on Selected Areas in Communications*, vol. 23, no. 2, pp. 201–220, 2005.

[6] F. K. Jondral, "Software-defined radio—basics and evolution to cognitive radio," *EURASIP Journal on Wireless Communications and Networking*, vol. 2005, no. 3, pp. 275–283, 2005.

[7] D. Čabrić and R. W. Brodersen, "Physical layer design issues unique to cognitive radio systems," in *Proceedings of the 16th IEEE International Symposium on Personal, Indoor and Mobile Radio Communications (PIMRC '05)*, pp. 759–763, Berlin, Germany, September 2005.

[8] Y. Xing, R. Chandramouli, S. Mangold, and S. S. N, "Dynamic spectrum access in open spectrum wireless networks," *IEEE Journal on Selected Areas in Communications*, vol. 24, no. 3, pp. 626–637, 2006.

[9] R. Tandra and A. Sahai, "SNR walls for feature detectors," in *Proceedings of the 2nd IEEE International Symposium on New Frontiers in Dynamic Spectrum Access Networks (DySPAN '07)*, pp. 559–570, Dublin, Ireland, April 2007.

[10] W. A. Gardner, *Cyclostationarity in Communications and Signal Processing*, IEEE Press, New York, NY, USA, 1993.

[11] W. A. Gardner, "Measurement of spectral correlation," *IEEE Transactions on Acoustics, Speech, and Signal Processing*, vol. 34, no. 5, pp. 1111–1123, 1986.

[12] M. Öner and F. K. Jondral, "Air interface recognition for a software radio system exploiting cyclostationarity," in *Proceedings of the 15th IEEE International Symposium on Personal, Indoor and Mobile Radio Communications (PIMRC '04)*, vol. 3, pp. 1947–1951, Barcelona, Spain, September 2004.

[13] T. Asai, A. Benjebbour, and H. Yoshino, "Recognition of CDMA signals with orthogonal codes using cyclostationarity," in *Proceedings of the 6th IEEE Workshop on Signal Processing Advances in Wireless Communications (SPAWC '05)*, pp. 480–484, New York, NY, USA, June 2005.

[14] M. K. Tsatsanis and G. B. Giannakis, "Transmitter induced cyclostationarity for blind channel equalization," *IEEE Transactions on Signal Processing*, vol. 45, no. 7, pp. 1785–1794, 1997.

[15] S. M. Kay, *Fundamentals of Statistical Signal Processing*, Prentice-Hall, Englewood Cliffs, NJ, USA, 1998.

[16] P. Marchand, J.-L. Lacoume, and C. Le Martret, "Multiple hypothesis modulation classification based on cyclic cumulants of different orders," in *Proceedings of the IEEE International Conference on Acoustics, Speech and Signal Processing (ICASSP '98)*, vol. 4, pp. 2157–2160, Seattle, Wash, USA, May 1998.

[17] A. Hauptschein and T. Knapp, "Maximum likelihood energy detection of M'ary orthogonal signals," *IEEE Transactions on Aerospace and Electronic Systems*, vol. 15, no. 2, pp. 292–299, 1979.

[18] F. F. Digham, M.-S. Alouini, and M. K. Simon, "On the energy detection of unknown signals over fading channels," *IEEE Transactions on Communications*, vol. 55, no. 1, pp. 21–24, 2007.

[19] M. Speth, S. A. Fechtel, G. Fock, and H. Meyr, "Optimum receiver design for OFDM-based broadband transmission. II. A case study," *IEEE Transaction on Communication*, vol. 49, no. 4, pp. 571–578, 2001.